Elastic Response of Graphene Nanodomes

Sascha Koch,[†,∥,*] Daniele Stradi,[‡,§,∥,*] Enrico Gnecco,[§] Sara Barja,[⊥,§] Shigeki Kawai,[†] Cristina Díaz,[‡] Manuel Alcamí,[‡] Fernando Martín,[‡,§] Amadeo Lopez Vázquez de Parga,[⊥,§] Rodolfo Miranda,[⊥,§] Thilo Glatzel,[†] and Ernst Meyer[†]

[†]Department of Physics, University of Basel, Klingelbergstr. 82, 4056 Basel, Switzerland, [‡]Departamento de Química, Universidad Autónoma de Madrid, Cantoblanco, 28049 Madrid, Spain, [§]Instituto Madrileño de Estudios Avanzados en Nanociencia (IMDEA Nanociencia), Cantoblanco, 28049 Madrid, Spain, and [⊥]Departemento de Física de la Materia Condensada, Universidad Autónoma de Madrid, Cantoblanco, 28049 Madrid, Spain. [∥]These authors contributed equally to this work.

ABSTRACT The mechanical behavior of a periodically buckled graphene membrane has been investigated by noncontact atomic force microscopy in ultrahigh vacuum. When a graphene monolayer is grown on Ru(0001), a regular arrangement of 0.075 nm high nanodomes forming a honeycomb lattice with 3 nm periodicity forms spontaneously. This structure responds in a perfectly reversible way to relative normal displacements up to 0.12 nm. Indeed, the elasticity of the nanodomes is proven by realistic DFT calculations, with an estimated normal stiffness $k \sim 40$ N/m. Our observations extend previous results on macroscopic graphene samples and confirm that the elastic behavior of this material is maintained down to nanometer length scales, which is important for the development of new high-frequency (terahertz) electromechanical devices.

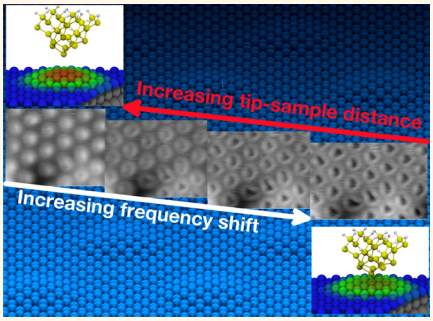

KEYWORDS: graphene · nanodomes · elastic response

The ability to produce single layers of graphene, the investigation of their physical and chemical properties, and their use in new devices is a topic of utmost importance.[1−3] One of the key features of graphene monolayers is their exceptional mechanical strength, with a remarkably high Young's modulus of the order of 1 TPa, as reported for free-standing membranes with linear sizes of tens to hundreds of micrometers.[4] This has allowed the development of electromechanical resonators with fundamental frequencies in the megahertz (MHz) regime.[5,6] Shrinking the linear size of the graphene membranes down to the nanometer range could boost the resonance frequency into the terahertz (THz) regime. To this end, it is essential to determine the mechanical properties of graphene at the nanoscale and, in particular, its elastic behavior.

When a monolayer graphene is grown on Ru(0001), a regular lattice of hills and valleys with 3 nm periodicity forms spontaneously,[7] originating a hexagonal pattern of 0.075 nm high nanodomes. The hills show quantum-dot-like localized electronic states, that is, an electronic structure that is different from the one at the valleys.[8] Here, we have characterized the mechanical response of this system using atomic force microscopy (AFM). The graphene elevations have been periodically indented by the probing tip, and the deformation is proven to be perfectly reversible. This conclusion is substantiated by realistic density functional theory (DFT) calculations, which confirm the elastic response of the nanodomes in this distance range. These results, combined with the peculiar local electronic structure of the nanodomes, suggest that the elastic properties of the nanodomes could be important for developing novel electromechanical nanodevices such as nanoresonators operating in the THz range.

The graphene monolayer has been grown epitaxially by thermal decomposition of ethylene on Ru(0001).[7] The carbon superstructure obtained in this way presents a high degree of perfection, as previously shown by scanning tunneling microscopy (STM) and by helium and X-ray diffraction.[9−11] In order to quantify the nanomechanical properties of this structure, we have used

* Address correspondence to sascha.koch@unibas.ch, daniele.stradi@uam.es.

Received for review August 26, 2012 and accepted March 8, 2013.

Published online March 08, 2013
10.1021/nn304473r

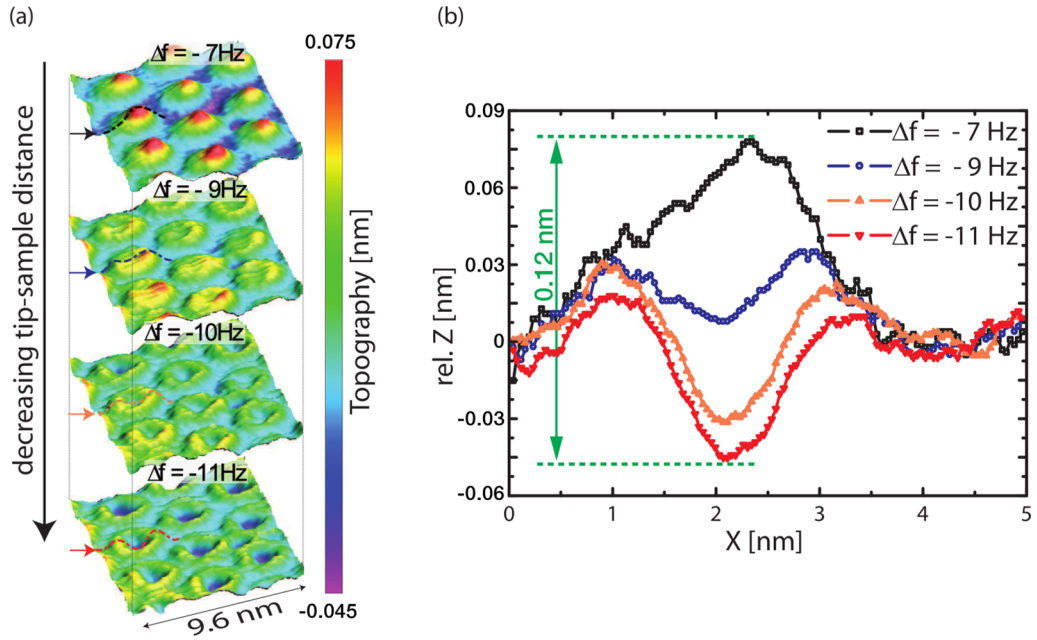

Figure 1. (a) Four AFM topographies (9.6 × 9.6 nm^2) recorded at different frequency shifts $\Delta f = -7, -9, -10$, and -11 Hz. The electrostatic force was continuously compensated while scanning. Parameters: amplitude = 8 nm, $U_{bias} = -512$ mV. The cross sections in (b), taken along the fast scan direction, show the elastic deformation of the hill sites marked by the corresponding colored lines in (a). The valley site of every curve is adjusted to rel. $Z = 0$ nm.

a home-built AFM under ultrahigh vacuum (UHV) conditions operated in the frequency modulated (FM) noncontact (NC) mode.[12,13] In this mode, the tip−sample relative distance is controlled by maintaining a constant shift of the probe resonance frequency with respect to the "free" value f_0. The frequency shift Δf is determined by the normal force F between probing tip and surface, and two-dimensional (2D) mapping of the force field experienced by the tip can thus be obtained by Z spectroscopy as discussed in the Methods section.[14,15] DFT calculations have been performed to simulate the tip−sample interaction at various distances, using a realistic supercell made of 11 × 11 graphene unit cells and a three-layer slab of 10 × 10 Ru(0001) unit cells for the substrate[16] and a well-tested model for the silicon tip.[17]

It is important to note that the periodic buckling of the graphene monolayer is a direct consequence of the mismatch between the lattice constant of Ru(0001) (0.27 nm) and that of graphene (0.24 nm). This originates a moiré pattern in the adlayer that repeats periodically every 3 nm. Depending on the particular atomic registry of the carbon atoms with respect to the ruthenium topmost layer, their mutual interaction changes radically. If the graphene atoms or the C−C bonds sit on top of a metal atom ("valley" site), the interaction with the metal is covalent and strong with a small (0.22 nm) average C−Ru distance.[11,18] Here, the graphene electronic structure is heavily modified by the underlying substrate. On the other hand, when the C ring is centered above a ruthenium atom ("hill" site), the interaction, mostly due to van der Waals forces,[16] is much weaker. The outcome of such strongly inhomogeneous environment is that the graphene layer tends to relax outward in the weakly bound areas, forming almost free-standing graphene nanodomes of about 0.1 nm in height. Due to the lateral confinement imposed by the different bonding characteristics of the surrounding areas, such hills are electronically decoupled from the rest of the surface, as demonstrated by the surface potential, which is ∼0.25 eV higher than in the valleys,[19] and by the appearance of localized electronic states both close to and well above the Fermi level.[7,8,20]

RESULTS AND DISCUSSION

Figure 1a shows four AFM topographies of the graphene superstructure simultaneously imaged with increasing absolute values of Δf (from −7 to −11 Hz) on the same area (using the "multipassing" acquisition procedure as discussed in the Methods section). Approaching the tip to the surface by using a more negative frequency shift changes considerably the topographies. The hills appear to be gradually compressed until they resemble nanopits. Further details can be inferred from the cross sections in Figure 1b. The undistorted hills (black curve) show an apparent height of about 0.075 nm with respect to the valley sites. This value is in accordance with the corrugation estimated by previous experiments[10] and calculations.[16] By further approaching the tip toward the graphene layer, the hill site is continuously indented, as shown by the blue, orange, and red cross sections, while the valley sites remain unchanged. The inner

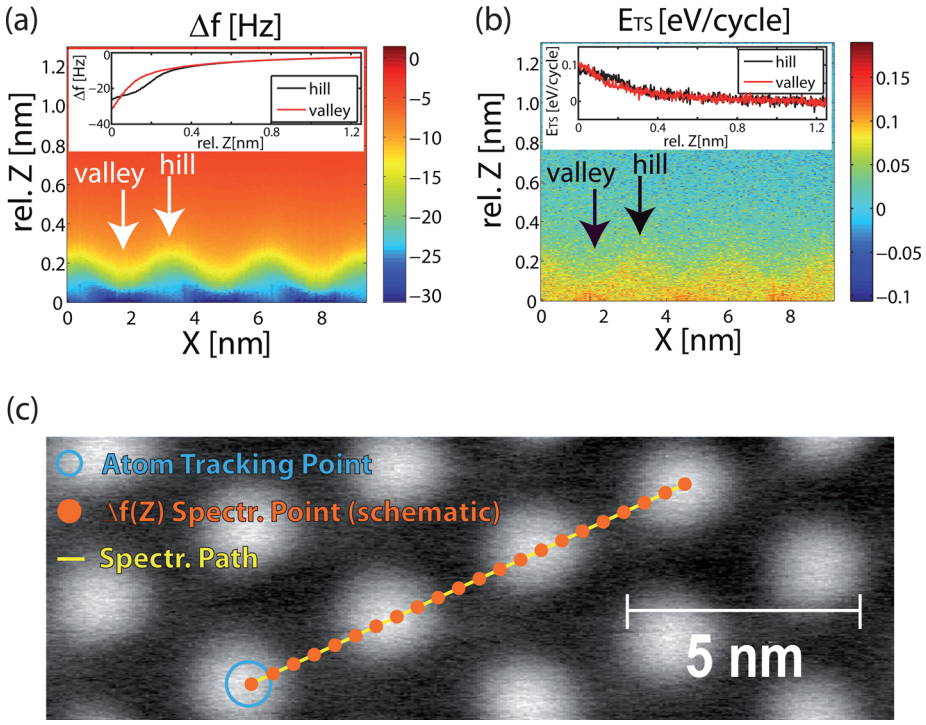

Figure 2. Two-dimensional spectroscopy plots of (a) frequency shift $\Delta f(Z)$ and (b) energy dissipation E_{ts}. The insets of (a) and (b) are site-dependent (hill, valley) 1D spectroscopy curves, extracted out of the 2D data, averaged over three curves. Parameters: amplitude = 7 nm, $U_{bias} = -819$. (c) Topographic NC-AFM image of the area used for 2D spectroscopy on the graphene/Ru(0001) subtrate. The yellow line represents the original spectroscopy path, while the blue circle is the tracked position for the AtomTracking function. The red dots are drawn schematically, representing the 128 Δf spectroscopy points with a resolution of 512 points each. Parameters: $\Delta f = -7$ Hz, amplitude = 8 nm, $U_{bias} = -556$ mV.

diameters of the nanopits formed by the tip indentation are about 2 nm, and the relative deformation in the Z direction reaches a maximum value of 0.12 nm (red curve), that is, almost twice the size of the apparent corrugation of the domes. The fact that the domes perfectly recover their initial shape after each scan suggests that their behavior under heavy deformation is reversible.

The 2D spectroscopy in Figure 2a presents the lateral distribution of the frequency shift, $\Delta f(Z)$, measured along the path indicated in Figure 2c. The inset shows the contrast inversion occurring at very small values of relative tip−sample distance ($Z < 0.15$ nm). At the minimum relative distance between the tip and the surface, the frequency shift on the hills is larger than on the valleys. Figure 2b shows the variation of the energy dissipation, E_{ts}, which accompanies the tip oscillations when the surface is approached. This quantity was estimated from the variation of the excitation amplitude A_{exc} of the microcantilever sustaining the probing tip, as compared to the value of the free excitation amplitude $A_{exc,0}$ applied when the tip is far from the surface:

$$E_{ts} = E_0\left(\frac{A_{exc}}{A_{exc,0}} - \frac{f}{f_{1st}}\right) \approx \frac{\pi k A^2}{Q}\left(\frac{A_{exc}}{A_{exc,0}} - 1\right) \quad (1)$$

In eq 1, E_0 represents the intrinsic loss of energy per oscillation cycle; f_{1st} is the resonance frequency of the first flexural mode of the cantilever; k is the cantilever spring constant, and Q and f_0 are the quality factor and resonance frequency of the free cantilever, respectively. Since $\Delta f \ll f_{1st}$, we have assumed that $f \approx f_{1st}$ in eq 1.[21] As a result, the dissipation turns out to be approximately the same on the valley and hill sites. The Z dependence shown in the inset in Figure 2b suggests that the dissipation is presumably due to Joule heating, caused by a charge modulation in tip or sample at large oscillation amplitude.[22]

To further investigate the process of contrast inversion, we have estimated the total normal force F between the tip and the sample out of the Δf signal by using the Sader−Jarvis method.[23] Figure 3a displays the force F as a function of the relative tip−sample distance. While on the valley sites the force F is attractive and continuously increases in modulus up to 0.5 nN with decreasing relative tip−surface distance Z, the hills respond differently: after first increasing to 0.3 nN, F then decreases and becomes less attractive. The crossing point in the inset curves for the hill and valley sites (marked by an arrow) represents the point of contrast inversion for the superstructure corrugation. Additional insight can be gained by subtracting the long-range van der Waals forces. These forces were estimated by fitting the Δf signal at large relative distances from the surface ($Z \geq 1$ nm), with a Hamaker-like model for the interaction of a spherical tip with an

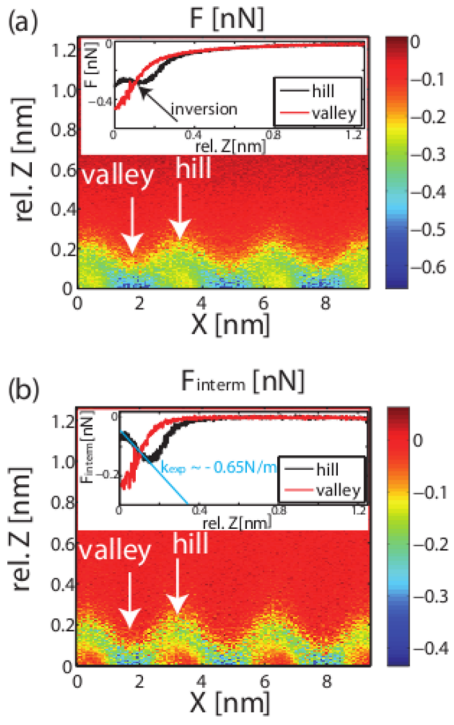

Figure 3. Two-dimensional spectroscopy plots along the same cross section of Figure 2: (a) total force *F* and (b) intermediate force F_{interm}. The insets in (a) and (b) are site-dependent (hill, valley) 1D spectroscopy curves, extracted out of the 2D data and averaged over three curves. The inversion point is again indicated by the crossing point of the hill and valley curves in the inset. Parameters: amplitude = 7 nm, U_{bias} = −819 mV.

infinite plane (note that since this method has been developed for atomically flat samples, it may be inaccurate in the present case, due to the corrugated nature of the graphene/Ru(0001) surface).[24] The vdW background so determined was subtracted from the $\Delta f(Z)$ data. The resulting curve (Figure 3b) represents the "intermediate" tip−surface force F_{interm}. This force is zero far away from the surface and, when the tip approaches the surface at a valley site, it becomes more and more attractive without changing its trend at the minimum relative distance (Z = 0.1 nm) that can be achieved without crashing the tip. In contrast, on top of a hill site, the attractive force F_{interm} peaks up to a maximum value of 0.15 nN at a relative distance of 0.2 nm. After that, it decreases almost linearly until F_{interm} = 0.08 nN at the minimum distance approach. From the slope of the F_{interm} *versus* Z curve, an overall force gradient of k_{exp} = 0.65 ± 0.4 N/m is estimated. Note that this value cannot be directly interpreted as the stiffness of the graphene membrane k_{dome} since k_{exp} also contains information on the gradient of the tip−sample interaction force and on the tip stiffness.[25,26]

The NC-AFM results show that the response of the hills to an external perturbation (by means of the probing tip) is qualitatively different from that of the valleys and suggest that the process is reversible in the former. As discussed above, the complex nature of the surface, the convolution of the information relative to the stiffness of both the tip and the sample, and their mutual interaction in the NC-AFM experiment prevent a quantitative analysis of the mechanical properties of the graphene nanodome based on the experimental data only. Therefore, extensive DFT calculations of the interaction between the graphene/Ru(0001) surface and a silicon nanotip were performed. These model simulations allow us to characterize the atomic-scale response of the surface upon interaction with a probing tip, without taking into account the complex dynamic problem involved in a NC-AFM experiment, which would be unattainable at the DFT level. The graphene/Ru(0001) surface is described using an 11 × 11/10 × 10 graphene/Ru(0001) supercell with three Ru layers[16] that accounts explicitly for the formation of the domes and is capable of reproducing several crucial experimental observations.[16,20] An asymmetric Si nanotip, based on the 2 × 1 Si(100) dimer reconstruction,[17] is employed. Indeed, it has been shown[27] that such a nanotip is capable of providing semiquantitative agreement with NC-AFM experiments at low temperature[28] on carbon nanostructures. Similarly to ref 27, we also include dispersion interactions[29] (for a more detailed description of the computational setup, see the Methods section).

Figure 4a shows the calculated $F(Z)$ curves over the hills (approach and retract) and valleys (approach) of the corrugated graphene/Ru(0001) superstructure, as well as the structures of the simulated indentation process on the hill at Z = 0.2 and 0.0 nm above the graphene (Figure 4b). It can be seen that the salient features observed in the experimental $F(Z)$ curves are consistent with theory. When the nanotip is far away from the surface (Z > 0.2 nm), the interaction is purely attractive, due to the background provided by vdW forces.[27] On the hills, the attraction increases up to the curve minimum (Z = 0.2 nm), where the force reaches a maximum value of 0.5 nN. Up to this point, the shape of the dome is hardly affected by the presence of the nanotip (see right inset in Figure 4a). A further approach of the tip to the surface (Z < 0.2 nm) leads to the onset of the repulsive forces, as evidenced by the abrupt change of sign of the $F(Z)$ curve slope. As the contribution of the repulsive forces becomes more and more important, the graphene dome starts to deform under the nanotip compression, reaching a maximum vertical deformation of 35 pm at Z = 0 nm (see left inset in Figure 4a). At Z < 0.2 nm, the tip also undergoes a progressive deformation in the direction opposite to that of the dome. The deformation increases with decreasing Z, reaching 42 pm at Z = 0 nm. On the other hand, the overall force on the valleys remains attractive (*i.e.*, $F \leq 0$ nN) over the whole range of tip−surface distances explored. Due to the superstructure corrugation, in this region, the onset of the repulsive

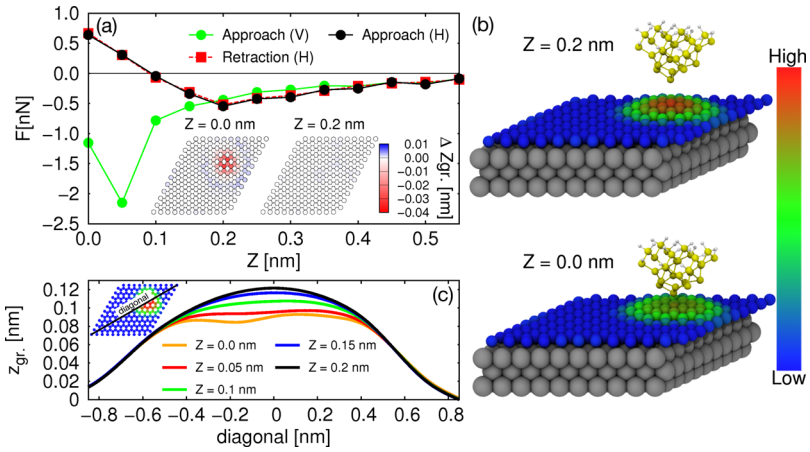

Figure 4. (a) Calculated force (*F*) *versus* distance (*Z*) curves for the hill site indentation (approach, black solid line; retraction, red dashed line) and *F*(*Z*) curve for tip approaching the valleys (green) of graphene/Ru(0001). (b) Optimized geometries at the minimum of the force curve on the hill site (top image, *Z* = 0.2 nm) and at maximum indentation (bottom image, *Z* = 0.0 nm). The inset in (a) shows the height variation (Δz_{gr}) of the graphene atoms with respect to the geometry optimized in the absence of the tip at the same two points of (b). Ru, Si, and H atoms are represented in silver, yellow, and white, respectively. C atoms of the graphene monolayer are shown in different colors depending on their height. (c) Profiles of the indented graphene hill (*Z* ≤ 0.2 nm) along the moiré unit cell diagonal. The zero on the *x*-axis is set at the central atom of the graphene dome. Each color is relative to a different value of *Z*.

forces occurs at a value of *Z* lower than in the hills (*Z* ≤ 0.1 nm). Therefore, at the onset of the repulsive forces over the hills (0.1 nm ≤ *Z* < 0.2 nm), the attractive forces in the valleys are still increasing. These results qualitatively reproduce the behavior observed in the experimental *F*(*Z*) curves, supporting the idea that the change of slope in the $F_{interm}(Z)$ curve over the hills can be associated with the mechanical deformation of the graphene dome. Figure 4c shows the profile of the graphene hill at different values of *Z*. It can be seen that the deformation is symmetric for relatively small deformations (0.1 nm ≤ *Z* < 0.2 nm) but becomes highly asymmetric at *Z* < 0.1 nm, due to the asymmetric character of the tip. Nevertheless, when the tip is retracted back to its initial position, the system recovers its initial shape, moving backward along the steps followed during the approach. This last observation, reflected in the absence of a hysteresis loop in the overall process (the approach and retraction curves overlap each other), confirms the reversibility of the indentation process.

Previous calculations[27] revealed that, for a nanotip interacting with both graphene and carbon nanotubes, the overall shape of the force *versus* distance curve is almost independent of the precise nanotip apex position. The small modulations, arising from the highest Pauli repulsion at the top sites with respect to hollow sites of the carbon lattice, were found to be important to determine the atomic-scale contrast, which is not of interest in the present work. In our case, the topmost region of the ripple, due to its weak coupling of graphene to the Ru(0001) surface, is likely to behave similarly to pristine graphene, with small variations of the tip−sample interaction among the different high-symmetry sites of the honeycomb. This consideration is also supported by the fact that the force *versus* distance curves shown in Figure 4a are very much like those calculated at the top site of pristine graphene.[27]

Some additional considerations have to be done regarding the possible influence of the position and orientation of the nanotip with respect to the underlying graphene hill. In some cases, the precise alignment of the nanotip can strongly influence its interaction with the surface.[30,31] In our case, we have checked for this by calculating the *F*(*Z*) curves for two additional alignments of the nanotip with respect to graphene. In our calculations, the nanotip is positioned over the graphene hill so that the lowest atom of the nanotip and the highest one of graphene are one on top of the other. For the results presented in Figure 4, the tip apex dimer is oriented antiparallel to one of the three C−C bonds connecting the highest graphene atom (see scheme named "Φ = 0°" in Figure 1 of the Supporting Information). Starting from this geometry, a rotation of the tip around the surface normal of 180 and 30° results in the apex dimer being oriented parallel to the graphene C−C bond and tilted by 150° with respect to the graphene C−C bond, respectively (see schemes "Φ = 180°" and "Φ = 30°" in Figure 1 of the Supporting Information). The *F*(*Z*) curves calculated for the Φ = 180 and 30° orientations of the tip (see Figure 1 of the Supporting Information) show a very similar behavior to those in Figure 4 and no hysteresis loop. Additionally, it can be noticed that for *Z* < 0.2 nm (*i.e.*, in the repulsive regime), the calculated force shows a monotonous increase going from the antiparallel to the parallel orientation. This can be associated with the increasing repulsion between the electron clouds of the dimer apex and the graphene since in this region

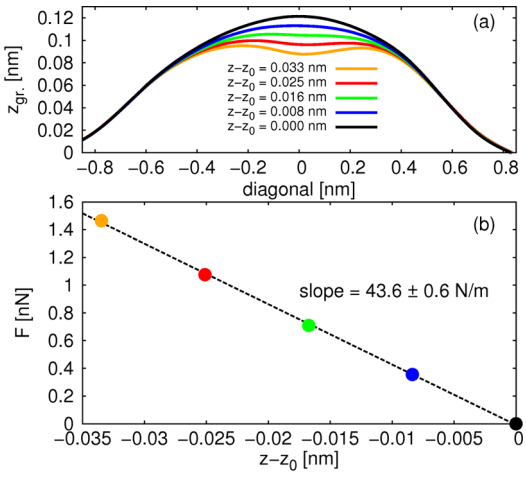

Figure 5. (a) Profile of the artificially deformed graphene hill along the simulation cell diagonal. The zero on the *x*-axis is set at the central atom of the graphene ripple. (b) Force on the central atom of the graphene ripple as a function of $z - z_0$. The different colors are relative to different values of $z - z_0$ (same colors in a and b). The dashed line is a linear fit to the data.

the interaction is dominated by the short-range repulsive forces. A representative example of this trend is the force calculated at $Z = 0.0$ nm, which changes from 0.64 nN for the antiparallel orientation to 1.10 nN for the parallel orientation. However, these small differences do not change the main result that the indentation maintains its reversible character independently of the precise nanotip orientation.

From a linear fit of the Z < 0.2 nm part of the $F(Z)$ curve calculated for the tip approaching the graphene hills, a force gradient $k_{DFT} = 7.6 \pm 1$ N/m is estimated for the tip−nanodome system. Due to the approximate description of the NC-AFM experiment provided by the calculations, this value is much higher than the corresponding value of k_{exp} experimentally determined in a distance range where the repulsive forces set on, but still do not prevail. As in the case of k_{exp}, k_{DFT} cannot be directly related to the elastic constant of the graphene dome. We have thus extracted the latter by performing a set of DFT calculations in which the graphene dome has been deformed artificially (*i.e.*, without the nanotip). This has been done by constraining the position of the central and highest atom of the graphene dome (having an initial position z_0) and displacing it stepwise of a quantity $z - z_0$ toward the ruthenium surface. This is equivalent to applying point-like load at the center of the graphene hill (see Figure 5a). The range of displacements considered (0 nm $\leq z - z_0 \leq$ 0.033 nm) is similar to that obtained during the simulations of the indentation of the dome. At each step, the structure has been relaxed and the component normal to the surface of the force acting on this atom has been calculated. The results (Figure 5b) show that the force increases linearly with the atom displacement $z - z_0$. From a fit of these data, a value of $k_{dome} = 43.6 \pm 0.5$ N/m has been extracted. This value can be compared with the stiffness $k_{cont} = 16\pi Eh^3/3R^2$ from classical elasticity theory,[32] where $h = 0.335$ nm is the monolayer thickness, $R = 1$ nm is the radius of the dome, and E is the Young's modulus of graphene. Taking the value $E = 1$ TPa from ref 4, $k_{cont} \sim 150$ N/m. Although the use of *continuum* mechanics is questionable for nanoscale graphene samples,[33] we can still use a classical formula to estimate the order of magnitude of the resonance frequency f_0 of the nanodomes. Assuming that the density of graphene is $\rho = 2.1 \times 10^{-3}$ kg/m^3, the frequency $f_0 \simeq (h/4R^2) \times (E/\rho^2)^{1/2}$ is expected to be on the order of 2 THz. This value can be further increased by tensile stresses.

CONCLUSION

In summary, the mechanical response of graphene nanodomes on Ru(0001) has been investigated by direct force measurements using noncontact atomic force microscopy. Topographical information using a multipassing procedure shows that the nanodomes are periodically indented by the probing tip. A maximum relative displacement ΔZ of about 0.012 nm is measured in the normal direction. Two-dimensional force spectroscopy strongly suggests that the deformation of the nanodomes is reversible. Density functional theory calculations with a quasi-static tip movement were performed down to much closer distances and verified the elastic response of the hill deformation. Since the expected resonance frequency of the nanodomes is in the same terahertz range as the frequency response of graphene transistors, these results can be exploited in the design of a new generation of nanoelectromechanical resonators.[5,6] They may also stimulate fundamental experimental and theoretical studies of mechanical properties of nonrigid surfaces. In particular, it would be quite interesting to apply scanning probe techniques such as force modulation[34] or contact resonance force microscopy[35] to characterize the mechanical response of the nanodomes when the forces between sample and probing tip are fully repulsive.

METHODS

Experimental Details. The graphene monolayer on Ru(0001)[7] was prepared under UHV conditions by cleaning a single crystal substrate by several cycles of 20 nm Ar-ion sputtering at 3×10^{-6} mbar and annealing at 1400 K for 40 min followed by an additional oxygen dosing (4×10^{-8} mbar, 1300 K, 40 min) and a final annealing at again 1400 K for 40 min. After this procedure, the temperature has been lowered to $T = 1300$ K,

and the ruthenium was exposed *in situ* to ethylene gas having a pressure $p = 10^{-7}$ mbar for 10 min. After stopping the exposure, the sample was heated again for 1 min at $T = 1400$ K and then cooled at room temperature.

The NC-AFM measurements were carried out in UHV at room temperature, employing highly n-doped silicon cantilevers with integrated tips as force sensors (Nanosensors: PPP-NCL). The typical resonance frequency and spring constant were $f_{first} = 170$ kHz and $k = 28$ N/m, respectively. The microscope was controlled by a Specs-Nanonis SPM controller in combination with two Specs-Nanonis OC4 PLL. The oscillation amplitude was set between 6 and 10 nm. The cantilevers were annealed for 30 min at 450 K, and the tip was cleaned by argon sputtering for 1−2 min at 680 eV with a gas pressure of 3×10^{-6} mbar. Two-dimensional force field spectroscopy[14,15] was performed using a dedicated LabView script, which controlled the Specs-Nanonis scanning software as well as the implemented AtomTracking function.[36,37] The 2D spectroscopy data were recorded along a straight line of 128 points on the graphene surface. Each of these points corresponds to a spectroscopy curve (512 points each) taken along the *Z* direction by reducing the tip−sample distance. In the insets of Figure 2 and Figure 3, the curves correspond to values averaged over three hill (black) and three valley (red) sites in the force map. Additionally, images at different set points (Δf) were recorded at each fast scan line (the so-called "multipassing function" in the Specs-Nanonis scanning software). During these measurements, amplitude modulated Kelvin force probe microscopy (AM-KFPM) was used for a continuous and reliable compensation of the local contact potential difference (CPD). In contrast, in the 2D force spectroscopy measurements, the CPD compensation of the electrostatic force was feasible at only one single point above the surface, where it was not possible to differ between the two contrast sites. Changing the relative tip−sample distance, the actual compensation voltage slightly differs from the CPD, leading to the observed dissipative Joule background. Since the time correlation is high, the thermal drift has no impact in the recorded data. The images were analyzed using the WSXM software.[38]

Computational Details. All of the calculations were performed using density functional theory (DFT), as implemented in Vasp.[39,40] The Perdew, Burke, and Ernzerhof (PBE) functional[41] was used. The vdW forces were taken into account by means of the DFT+D2 method.[29] Due to the dimensions of the supercell employed, the sampling of the Brillouin zone was restricted to the Γ-point. The tip was initially positioned at the center of the hill (valley) with its lowest atom lying above the carbon atom at the Ru(0001) hollow site. On the valley, we verified that, in the region of the *F*(*Z*) curve explored by the experiment (*i.e.*, when $F \geq 0$ nN), the behavior of the calculated *F*(*Z*) curve is independent of the precise tip position. In both cases (hill and valley), the tip was initially positioned with its lowest atom lying 0.8 nm above the highest one of graphene. Therefore, on the hill (valley), the initial tip−sample distance is 0.8 nm (0.92 nm). This shift reflects the one between the force *versus* distance curves measured on the hills and the valleys, obtained by matching the tails of the experimental force *versus* distance curve (0.093 nm). The force *versus* distance curves were calculated using a stepwise, quasi-static approach, moving the tip of 0.05 nm at each step, and relaxing the lowest 15 atoms of the tip, together with graphene and the topmost Ru layer. The convergence criterion for the forces was set to 0.01 eV/Å. The force acting on the tip at each step was calculated summing up the vertical forces on the tip atoms that were not allowed to relax.

Conflict of Interest: The authors declare no competing financial interest.

Acknowledgment. This work was supported by the Swiss National Science Foundation, the NCCR "Nanoscale Science" of the Swiss National Science Foundation, the Eurocores project FANAS, the Spanish MICINN through projects FIS2010-18847, FIS2010-15127, CTQ2010-17006, MAT3011-26312, and CONSOLIDER-INGENIO 2010 on Molecular Nanoscience as well as the CM program NANOBIOMAGNET S2009/MAT1726. Additionally, S.B. would like to acknowledge the FPU Grant AP-2007-001157 and Daniele Stradi the UAM-FPI program. The authors thank Lev Kantorovich for critical reading of the manuscript and clarifying comments.

Supporting Information Available: Calculated *F*(*Z*) curves for $\Phi = 180$ and 30° orientations of the nanotip, schemes showing the nanotip orientation in the calculated *F*(*Z*) curves for $\Phi = 0$, 180, and 30°, and movie of the calculated nanoindentation process for $\Phi = 0°$. This material is available free of charge *via* the Internet at http://pubs.acs.org.

REFERENCES AND NOTES

1. Novoselov, K. S.; Geim, A. K.; Morozov, S. V.; Jiang, D.; Zhang, Y.; Dubonos, S. V.; Grigorieva, I. V.; Firsov, A. A. Electric Field Effect in Atomically Thin Carbon Films. *Science* **2004**, *306*, 666–669.
2. Geim, A. K.; Novoselov, K. S. The Rise of Graphene. *Nat. Mater.* **2007**, *6*, 183–191.
3. Lin, Y.-M.; Dimitrakopoulos, C.; Jenkins, K. A.; Farmer, D. B.; Chiu, H.-Y.; Grill, A.; Avouris, P. 100-GHz Transistors from Wafer-Scale Epitaxial Graphene. *Science* **2010**, *327*, 662.
4. Lee, C.; Wei, X.; Kysar, J. W.; Hone, J. Measurement of the Elastic Properties and Intrinsic Strength of Monolayer Graphene. *Science* **2008**, *321*, 385–388.
5. Bunch, J. S.; van der Zande, A. M.; Verbridge, S. S.; Frank, I. W.; Tanenbaum, D. M.; Parpia, J. M.; Craighead, H. G.; McEuen, P. L. Electromechanical Resonators from Graphene Sheets. *Science* **2007**, *315*, 490–493.
6. Chen, C.; Rosenblatt, S.; Bolotin, K. I.; Kalb, W.; Kim, P.; Kymissis, I.; Stormer, H. L.; Heinz, T. F.; Hone, J. Performance of Monolayer Graphene Nanomechanical Resonators with Electrical Readout. *Nat. Nanotechnol.* **2009**, *4*, 861–867.
7. Vázquez de Parga, A. L.; Calleja, F.; Borca, B.; Passeggi, M. C. G.; Hinarejos, J. J.; Guinea, F.; Miranda, R. Periodically Rippled Graphene: Growth and Spatially Resolved Electronic Structure. *Phys. Rev. Lett.* **2008**, *100*, 056807-1–056807-4.
8. Borca, B.; Barja, S.; Garnica, M.; Sánchez-Portal, D.; Silkin, V. M.; Chulkov, E. V.; Hermanns, C. F.; Hinarejos, J. J.; Vázquez de Parga, A. L.; Arnau, A.; *et al.* Potential Energy Landscape for Hot Electrons in Periodically Nanostructured Graphene. *Phys. Rev. Lett.* **2010**, *105*, 036804-1–036804-4.
9. Borca, B.; Barja, S.; Garnica, M.; Hinarejos, J. J.; de Parga, A. L. V.; Miranda, R.; Guinea, F. Periodically Modulated Geometric and Electronic Structure of Graphene on Ru(0001). *Semicond. Sci. Technol.* **2010**, *25*, 034001–034008.
10. Martoccia, D.; Björck, M.; Schlepütz, C. M.; Brugger, T.; Pauli, S. A.; Patterson, B. D.; Greber, T.; Willmott, P. R. Graphene on Ru(0001): A Corrugated and Chiral Structure. *New J. Phys.* **2010**, *12*, 043028–043039.
11. Moritz, W.; Wang, B.; Bocquet, M.-L.; Brugger, T.; Greber, T.; Wintterlin, J.; Günther, S. Structure Determination of the Coincidence Phase of Graphene on Ru(0001). *Phys. Rev. Lett.* **2010**, *104*, 136102-1–136102-4.
12. Howald, L.; Meyer, E.; Lüthi, R.; Haefke, H.; Overney, R.; Rudin, H.; Güntherodt, H. J. Multifunctional Probe Microscope for Facile Operation in Ultrahigh Vacuum. *Appl. Phys. Lett.* **1993**, *63*, 117–119.
13. Albrecht, T. R.; Grütter, P.; Horne, D.; Rugar, D. Frequency Modulation Detection Using High *Q* Cantilevers for Enhanced Force Microscope Sensitivity. *J. Appl. Phys.* **1991**, *69*, 668–673.
14. Hölscher, H.; Langkat, S. M.; Schwarz, A.; Wiesendanger, R. Measurement of Three-Dimensional Force Fields with Atomic Resolution Using Dynamic Force Spectroscopy. *Appl. Phys. Lett.* **2002**, *81*, 4428–4430.
15. Schirmeisen, A.; Weiner, D.; Fuchs, H. Single-Atom Contact Mechanics: From Atomic Scale Energy Barrier to Mechanical Relaxation Hysteresis. *Phys. Rev. Lett.* **2006**, *97*, 136101-1–136101-4.
16. Stradi, D.; Barja, S.; Díaz, C.; Garnica, M.; Borca, B.; Hinarejos, J. J.; Sánchez-Portal, D.; Alcamí, M.; Arnau, A.; Vázquez de Parga, A. L.; *et al.* Role of Dispersion Forces in the Structure of Graphene Monolayers on Ru Surfaces. *Phys. Rev. Lett.* **2011**, *106*, 186102-1–186102-4.

17. Pou, P.; Ghasemi, S. A.; Jelinek, P.; Lenosky, T.; Goedecker, S.; Perez, R. Structure and Stability of Semiconductor Tip Apexes for Atomic Force Microscopy. *Nanotechnology* **2009**, *20*, 264015–264025.
18. Wang, B.; Bocquet, M.-L.; Marchini, S.; Gunther, S.; Wintterlin, J. Chemical Origin of a Graphene Moiré Overlayer on Ru(0001). *Phys. Chem. Chem. Phys.* **2008**, *10*, 3530–3534.
19. Brugger, T.; Günther, S.; Wang, B.; Dil, J. H.; Bocquet, M.-L.; Osterwalder, J.; Wintterlin, J.; Greber, T. Comparison of Electronic Structure and Template Function of Single-Layer Graphene and a Hexagonal Boron Nitride Nanomesh on Ru(0001). *Phys. Rev. B* **2009**, *79*, 045407-1–045407-6.
20. Stradi, D.; Barja, S.; Díaz, C.; Garnica, M.; Borca, B.; Hinarejos, J. J.; Sánchez-Portal, D.; Alcamí, M.; Arnau, A.; Vázquez de Parga, A. L.; *et al.* Electron Localization in Epitaxial Graphene on Ru(0001) Determined by Moiré Corrugation. *Phys. Rev. B* **2012**, *85*, 121404-1–121404-5.
21. Anczykowski, B.; Gotsmann, B.; Fuchs, H.; Cleveland, J.; Elings, V. How To Measure Energy Dissipation in Dynamic Mode Atomic Force Microscopy. *Appl. Surf. Sci.* **1999**, *140*, 376–382.
22. Denk, W.; Pohl, D. W. Local Electrical Dissipation Imaged by Scanning Force Microscopy. *Appl. Phys. Lett.* **1991**, *59*, 2171–2173.
23. Sader, J. E.; Jarvis, S. P. Accurate Formulas for Interaction Force and Energy in Frequency Modulation Force Spectroscopy. *Appl. Phys. Lett.* **2004**, *84*, 1801–1803.
24. Guggisberg, M.; Bammerlin, M.; Loppacher, C.; Pfeiffer, O.; Abdurixit, A.; Barwich, V.; Bennewitz, R.; Baratoff, A.; Meyer, E.; Güntherodt, H.-J. Separation of Interactions by Noncontact Force Microscopy. *Phys. Rev. B* **2000**, *61*, 11151–11155.
25. García, R.; Pérez, R. Dynamic Atomic Force Microscopy Methods. *Surf. Sci. Rep.* **2002**, *47*, 197–301.
26. Giessibl, F. J. Advances in Atomic Force Microscopy. *Rev. Mod. Phys.* **2003**, *75*, 949–984.
27. Ondráček, M.; Pou, P.; Rozsíval, V.; González, C.; Jelínek, P.; Pérez, R. Forces and Currents in Carbon Nanostructures: Are We Imaging Atoms? *Phys. Rev. Lett.* **2011**, *106*, 176101-1–176101-4.
28. Ashino, M.; Schwarz, A.; Behnke, T.; Wiesendanger, R. Atomic-Resolution Dynamic Force Microscopy and Spectroscopy of a Single-Walled Carbon Nanotube: Characterization of Interatomic van der Waals Forces. *Phys. Rev. Lett.* **2004**, *93*, 136101-1–136101-4.
29. Grimme, S. Semiempirical GGA-Type Density Functional Constructed with a Long-Range Dispersion Correction. *J. Comput. Chem.* **2006**, *27*, 1787–1799.
30. Sweetman, A.; Jarvis, S.; Danza, R.; Bamidele, J.; Gangopadhyay, S.; Shaw, G. A.; Kantorovich, L.; Moriarty, P. Toggling Bistable Atoms *via* Mechanical Switching of Bond Angle. *Phys. Rev. Lett.* **2011**, *106*, 136101-1–136101-4.
31. Jarvis, S.; Sweetman, A.; Bamidele, J.; Kantorovich, L.; Moriarty, P. Role of Orbital Overlap in Atomic Manipulation. *Phys. Rev. B* **2012**, *85*, 235305-1–235305-5.
32. Landau, L. D.; Lifshitz, L. M. *Theory of Elasticity*; Butterworth-Heinemann: Oxford, UK, 1986.
33. Tapasztó, L.; Dumitriča, T.; Kim, S. J.; Nemes-Incze, P.; Hwang, C.; Biró, L. P. Breakdown of *Continuum* Mechanics for Nanometre-Wavelength Rippling of Graphene. *Nat. Phys.* **2012**, *8*, 739–742.
34. Maivaldt, P.; Butt, H. J.; Gould, S. A. C.; Prater, C. B.; Drake, B.; Gurley, J. A.; Elings, V. B.; Hansma, P. K. Using Force Modulation To Image Surface Elasticities with the Atomic Force Microscope. *Nanotechnology* **1991**, *2*, 103–106.
35. Yamanaka, K.; Maruyama, Y.; Tsuji, T.; Nakamoto, K. Resonance Frequency and *Q* Factor Mapping by Ultrasonic Atomic Force Microscopy. *Appl. Phys. Lett.* **2001**, *78*, 1939–1941.
36. Pohl, D. W.; Möller, R. Tracking Tunneling Microscopy. *Rev. Sci. Instrum.* **1988**, *59*, 840–842.
37. Kawai, S.; Glatzel, T.; Koch, S.; Baratoff, A.; Meyer, E. Interaction-Induced Atomic Displacements by Drift-Corrected Dynamic Force Spectroscopy. *Phys. Rev. B* **2011**, *83*, 035421-1–035421-7.
38. Horcas, I.; Fernandez, R.; Rodriguez, J. M. G.; Colchero, J.; Herrero, J. G.; Baro, A. M. WSXM: A Software for Scanning Probe Microscopy and a Tool for Nanotechnology. *Rev. Sci. Instrum.* **2007**, *78*, 013705.
39. Kresse, G.; Hafner, J. *Ab Initio* Molecular Dynamics for Liquid Metals. *Phys. Rev. B* **1993**, *47*, 558–561.
40. Kresse, G.; Joubert, D. From Ultrasoft Pseudopotentials to the Projector Augmented-Wave Method. *Phys. Rev. B* **1999**, *59*, 1758–1775.
41. Perdew, J. P.; Burke, K.; Ernzerhof, M. Generalized Gradient Approximation Made Simple. *Phys. Rev. Lett.* **1996**, *77*, 3865–3868.